SCIENCE CHINA
Physics, Mechanics & Astronomy

• Article •

April 2015 Vol. 58 No. 4: 046801
doi: 10.1007/s11433-014-5623-x

The concept and realization of nanostructure fabrication using free-standing metallic wires with rapid thermal annealing

CUI AJuan[1], HAO TingTing[1], LI WuXia[1*], SHEN TieHan[2], LIU Zhe[1], JIANG QianQing[1] & GU ChangZhi[1,3*]

[1] *Beijing National Laboratory of Condensed Matter Physics, Institute of Physics, Chinese Academy of Sciences, Beijing 100190, China;*
[2] *Joule Physics Laboratory, School of CSE, College of Science and Technology, University of Salford, M5 4WT, UK;*
[3] *Collaborative Innovation Center of Quantum Matter, Beijing 100871, China*

Received August 27, 2014; accepted October 29, 2014; published online December 12, 2014

Free-standing metallic nanostructures are considered to be highly relevant to many branches of science and technology with applications of three dimensional metallic nanostructures ranging from optical reflectors, actuators, and antenna, to free-standing electrodes, mechanical, optical, and electrical resonators and sensors. Strain-induced out-of-plane fabrication has emerged as an effective method which uses relaxation of strain-mismatched materials. In this work, we report a study of the thermal annealing-induced shape modification of free-standing nanostructures, which was achieved by introducing compositional or microstructural nonuniformity to the nanowires. In particular gradient, segmented and striped hetero-nanowires were grown by focused-ion-beam-induced chemical vapor deposition, followed by rapid thermal annealing in a N_2 atmosphere. Various free-standing nanostructures were produced as a result of the crystalline/grain growth and stress relief.

thermal annealing, strain-induced deformation, free-standing, three-dimensional nanofabrication

PACS number(s): 81.40.Gh, 81.40.Ef, 81.40.Lm, 81.05.Bx

Citation: Cui A J, Hao T T, Li W X, et al. The concept and realization of nanostructure fabrication using free-standing metallic wires with rapid thermal annealing. Sci China-Phys Mech Astron, 2015, 58: 046801, doi: 10.1007/s11433-014-5623-x

1 Introduction

Electronic devices such as metal oxide semiconductor field effect transistor are usually planar in structure and essentially two dimensional. Recent trend in transistor scaling has already led to a change in gate structure from two to three dimensional, to minimize problems inherent in miniaturization [1], while work on 3D micro/nanostructures and nanodevices has shown excellent mechanical and physical properties as well as potential applications in optoelectronic devices [2], nanosensors [3], biological information detectors [4], plasmonics [5], and quantum devices [6], where planar structures are considered less favorable.

Various techniques and methods have been developed to fabricate 3D nanostructures, including (1) 3D structure fabrication by conventional micro/nanofabrication technologies, such as shadow evaporation [7], multilayer electroplating [8], membrane projection lithography [9], stress driven assembly [10], laser direct writing [11,12], and focused-ion-beam (FIB) induced chemical vapor deposition(CVD); (2) 3D structures made of nanowire bending [13–15]; and (3) other shape modifications [16–20]. Among them, recent studies on the post-growth shape manipulation of free-standing nanowires by ion beam irradiation [13–15] have shown good flexibility and controllability in 3D nanoshaping. The bending angle of an irradiated nanoobject can be well controlled by the kinetic energy, fluence, and the inci-

* Correspondence author (LI WuXia, email: liwuxia@aphy.iphy.ac.cn; GU ChangZhi, email: czgu@aphy.iphy.ac.cn)

dent angle of the ion beam. The shape modification of nanowires/sheets can be driven by a number of mechanisms, including thin film stress [16], surface tension [17], inflating and deflating balloon joints [18], swelling of electroactive polymers [19], and magnetic interaction [20]. The size of the structures fabricated using some of the methods, such as swelling of electroactive polymers and magnetic interaction, so far is limited to at least of an order of a micron [21]. For thin film stress and surface tension related-methods, to bend the object, specific processes are required and the procedure at present appears to be relatively complicated.

Previously, we have used FIB-induced CVD to grow Pt nanowires, which have a degree of microstructural and chemical compositional gradient across the diameter of the nanowries [22]. Followed by thermal annealing, point-contact and free-standing 3D microcages have been fabricated through bending of the vertical nanowires. In this work, we demonstrate the use of rapid thermal annealing (RTA) to achieve shape modification of 'bimetallic' nanowires or segmented nanowires made of dissimilar materials that would not be feasible through conventional lithography. Such structures can be produced in registration with each other and may be easily aligned with other electronic devices on the substrate. Namely, gradient, striped, and segmented heterostructures were grown by FIB-induced CVD and followed by thermal annealing to produce free-standing structures. The relative mechanisms are discussed.

2 Background and experimental

2.1 The concept of basic thermally induced deformation modes of nanowires

The bending behaviors of free-standing nanowires upon thermal annealing are schematically shown in Figure 1. In principle, by introducing thermal annealing to a homogeneous free-standing object, strain relaxation, and microstructure changes in different parts are uniform. Thus the object is expected to undergo no shape changing as shown in Figure 1(a). However, if there are some predefined profiles of variation across the object in terms of the strain, the defect density, the chemical composition, or the microstructure, thermal annealing could cause the "gradient" object deformation as shown in Figure 1(b), owing to the possible relaxation of strain/stress, or uneven recrystallization, or uneven grain growth. Also, striped nanowires, which are formed with two different materials with large difference in the thermal expansion coefficient, would undergo bending when annealed as shown in Figures 1(c)–(e). By a judicious choice of a combination of the striped or gradient segments, or various shapes can be achieved to form complex free-standing nanostructures.

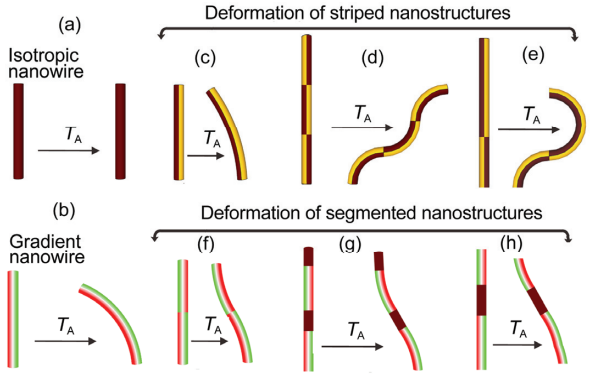

Figure 1 (Color online) An illustration of the deformation mechnism of free-standing nanoobjects upon thermal annealing: (a) isotropic nanowires undergo no bending; (b) nanowires with anisotropic cross-sections bend when annealed; (c)–(h) striped and segmented heterostructures bend with design shape and configuration when annealed.

2.2 Growth of hybrid nanowire structures

First various nanowire structures were examined. For clarity, Type A structure refers to FIB-grown tungsten (W) composite nanowires, which show no bending after annealing; Type B structure refers to FIB-grown platinum (Pt) composite nanowires, which are believed to have compositional and structural gradients across the diameter and bend when annealed; Type C structures have striped A/B configuration ("bimetallic"), which have Pt composite deposited along one side of the W nanowires and are expected to bend when annealed. Such unit can also be arranged in the segmented form, for instance, A/B followed by B/A, then A/B and then B/A and so on along the axis of the structure. The length of each segment may also be varied; type D structures refer to those composed of units of different segments, for instance, stacks of A-B segments. The Pt and W composite materials were grown by FIB-induced CVD with $(CH_3)_3Pt$ ($CpCH_3$) and $W(CO)_6$ as precursors, respectively. The growth systems used are dual beam FIB/scanning electron microscopes (SEM) (FEI DB 235 and Helios 600i). The ion column has a singly charged liquid gallium ion source, which is placed at an angle of 52° to the vertically oriented electron beam column.

Vertically free-standing hybrid nanowires were grown site-specifically in a single step using a gas injection system installed in the dual beam FIB/SEM facilities. During growth, gases were delivered to the sample surface in close proximity to the surface (~50–150 μm) through the precursor nozzle, whereas the FIB was scanned by the "spot-mode". In such a scanning strategy, an ion beam current of 1 pA with a nominal diameter of 7 nm was kept stationary in a particular position. The sample chamber pressure was about 10^{-5}–10^{-6} mbar during deposition. The FIB-induced CVD process is known to have involved the adsorption of gas molecules on substrate, dissociation/decomposition of gas molecules by the ion beam, resulted in the deposition of the material as well as removal of the organic ligands, and each step being controlled by different growth parameters [23]. The shape and size, chemical composition, and micro-

structure of a material grown by FIB-assisted CVD are largely related to the precursor nozzle position, the ion beam current density, the ion beam scanning procedure, the growth temperature, the supporting substrate, and the types of the gas precursor used during growth. The use of a single precursor nozzle has been shown to introduce the desirable bending effect [22]. According to the dynamics of the growth mechanism [23], the deposition rate is mainly limited by two factors and can be divided into two regimes. They are the current limited regime within which the growth rate is independent of the gas flux, and the gas flux limited regime within which the growth rate is independent of the current density [23]. In both regimes, the growth rate increases linearly with the dwell time, the time duration in which that the scanning beam stays in a particular location. In the case of using ion beam current of 1 pA with spot size of a few nanometers, the corresponding current density was about 1.6×10^{19} charge s^{-1} cm^{-2}. Thus, when the precursor gas molecules are provided by using a single gas injection nozzle with the beam scanned on one side of the gas injection nozzle, the gas flux is no longer rotationally symmetric about the point of growth. Pt growth using such conditions is likely to induce compositional nonuniformity along the diameter, but maintaining homogeneity along the axis of the wire.

The length of a wire or a segment was controlled by the deposition time. Segmented nanowires were grown by changing the gas precursors in turn in the spot mode, while striped nanowires were grown using a line pattern, which was positioned on one side of a previously grown nanowire with a different gas precursor to that used for the growth of the host nanowire. Also, by rotating the sample stage, the relative position of each wire to the gas nozzle can be precisely adjusted, through which the bending direction of the nanowire upon annealing was controlled.

2.3 Thermal annealing treatment and deformation characterization

In this work, thermal annealing treatments were conducted in a RTA furnace purged with a constant flow of N_2 gas. For each individual treatment, the temperature was increased to the setting value in about 20 s and it was then kept for 60 s. In the purged N_2 atmosphere, N_2 gas flow rate was 10.0 standard liters per minute (slpm). The use of N_2 purge was to reduce the effect of oxidation during annealing. The annealing cycle number and annealing temperatures were varied. After each thermal treatment, the specimen was transferred to an SEM for imaging, which was used for deformation analysis.

3 Results and discussions

3.1 Thermally induced bending of composite nanowires

First, Type B structures, a serial of vertically grown Pt composite nanowires of the same diameter (243 nm) but different heights (8.2, 7.1, 6.1, 5.4, 4.6 and 3.6 μm) were fabricated to investigate the influence of the annealing temperature (T_A) on the bending process. Figure 2(a) shows the angle deviation from vertical as a function of the annealing temperature, each wire was rapid thermal annealed with T_A increased from 500°C to 900°C by a step size of 100°C and each individual annealing cycle lasted for 60 s in a purged N_2 atmosphere, with a N_2 gas flow rate of 10.0 slpm. Consistent with the results reported in ref. [22], nanowires again were observed to have a uniform bending over their entire length. It can be seen from the SEM images in the inset that all wires bent pointing towards the precursor nozzle. Figure 2(b) shows that higher annealing temperature results in large extent of deformation of the nanowires. Also, at a particular annealing temperature, by increasing the annealing time (annealing number), nanowires can be deformed more and they finally saturate. The reasons for this behavior can be found elsewhere [22]. Figure 2(c) shows that Pt nanowires grown by FIB-induced CVD can also be bent in the lower temperature region. In the lower temperature region, there was a little thermally induced shape modification, but with increasing T_A, the bending increased significantly. Figure 2(d) shows the bending of focused-electron-beam (FEB)-induced deposition of Pt nanowires when annealed in N_2 atmosphere. All these results illustrate that curved architectures can be achieved by bending of composite Pt nanowires grown by FEB- or FIB- induced deposition.

In our earlier work, it has been observed that for a FIB-

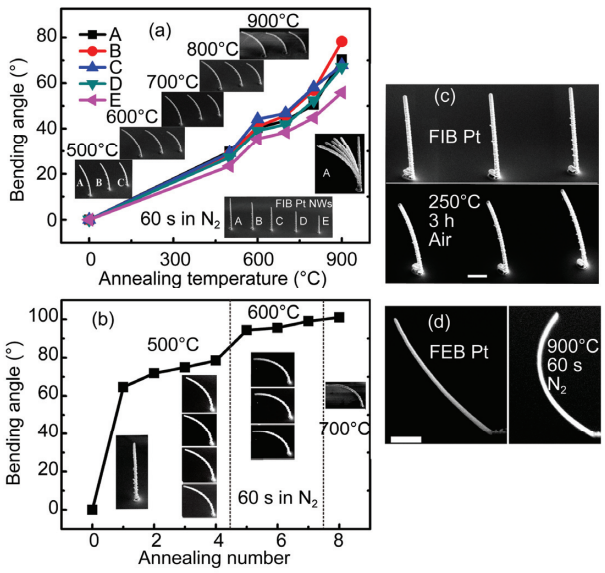

Figure 2 (Color online) (a) the bending angle (the deviation from vertical) of Pt composite nanowires (type B) as a function of the annealing temperature, in the inset is the SEM image of selected naowires before and after annealing; (b) the annealing number-dependent bending angle of wire annealed at some particular temperatures; (c) mild bending of FIB-Pt nanowires at 250°C; and (d) annealing of FEB-Pt in N_2 under 900°C. The scale bars represent 1 μm, and the SEM images were taken at room temperature.

grown Pt nanowires, the bending obeys a linear relationship between the bending curvature θ and the length of the wire L [22]. In that, the wire length dependent bending can be quantified by an expansion coefficient difference across the diameter of the wire during bending and the bending angle should be proportional to the wire length L for nanowires having the same diameter, which agrees well with the experimental observation shown in Figure 2. It can also be seen that substantial bending of the nanowires occurred during the initial annealing cycle with annealing temperature of 500°C, with smaller amounts of additional bending, and finally saturated in subsequent annealing cycles. However, when T_A increased, the bending angle jumped to a higher value, and there is only a small amount of extra bending at this temperature till it saturates again. The arch shape bending is mainly due to the difference in the expansion coefficient across the wire diameter, which can well be due to the variation in the chemical composition: the carbon content was found to be higher on side of the wires closer to the precursor nozzle whilst Pt content was higher on the opposite side with relatively smaller crystallographic domains in the side closer to the gas injector. After annealing, the Pt grains increased in size and the degree of increment and crystallization are larger on the side further away from the gas injection nozzle. The observations have been reported elsewhere [22]. It is the difference in the expansion coefficient on the two sides that is responsible for anisotropic macroscopic deformation of the gradient nanowires, that is, bending toward the injector.

Also, since defects or atomic diffusion, recrystallization, and grain growth are likely to be closely dependent on annealing time and temperature, the bending process is different for structures annealed using different annealing processes. For instance, grain growth involves short-range diffusion and the extent of recrystallization depends on both temperature and time. Further grain growth can occur when crystalline material is maintained at a certain annealing temperature and complete recrystallization can be achieved by increasing the annealing time. Slow temperature ramping rate could result in mild and gradual bending or deformation of the structures since structural differences, such as quenching in the vacancy concentration and alerting of the free volume, are largely heat cycling related. Such processes are irreversible. Therefore, the shape changes are plastic in nature. Changes in the spatial distribution of compositional and structural short-range order have been observed in FIB-grown Pt composite upon annealing of the amorphous phase [22].

3.2 Bending of striped nanostructures

To fabricate Type C structures, a W nanowire was first deposited, then the stage was tilted with the ion beam 45° grazing incident to the length direction of the wire, then Pt composite was deposited. For comparison, thermal treatment was conducted on W vertical nanowires and striped A/B structures with different sizes of the deposited Pt strips. Figures 3(a)–(c) show the SEM images of the as-deposited and annealed W composite nanowires, striped W/Pt structures, and partially striped W/Pt structures, respectively. Bending was observed when annealed though W composite nanowire did not bend itself. Also, the striped wire always bend in a way that Pt is on the outer arc and W the inner arc, which happens irrespective of the injector position for the growth of Pt. This might suggest that the material difference overwrites the effect associated with single Pt wire.

These behaviors may be explained by the difference in the properties of the grown materials. SEM imaging reveals that the focused-ion-beam-induced deposition rate of W (by spot mode for nanowire growth) was about one-fourth of that of the Pt composite with smoother surface. Also, high resolution transmission electron microscope characterization indicates that FIB-grown W and Pt composites both have fine W or Pt crystalline grains embedded in C matrix, while the size of W grains is a few times smaller than that of the Pt grains. These factors suggest possible larger uneven chemical composition, strain, and defect distributions across the diameter of the FIB-grown Pt nanowires. In addition, the thermal expansion coefficient of bulk W is about half of that of the Pt. Although thermal expansion itself could be elastic, the elastic deformation could contribute and enhance the irreversible grain growth/crystallization during the thermal treatment [24,25].

Curved structures, even tubes have been formed by releasing micro-sized bilayer thin films that have different lattice constants from substrate. The residual stress in the system due to a lattice mismatch between each layers acts as the driving force for the bending [26]. However, the Pt and W composite materials in our work are amorphous. They are composites and only the portions that have Pt deposited bent; and the wider the deposited Pt strip, the more the whole structure bent, as can be seen in Figure 3(c). This is consistent with the diameter-dependent bending behavior of FIB-grown gradient Pt nanowires [22].

3.3 Deformation of Pt–W-segmented nanowires

The annealing number (time)-related deformation process

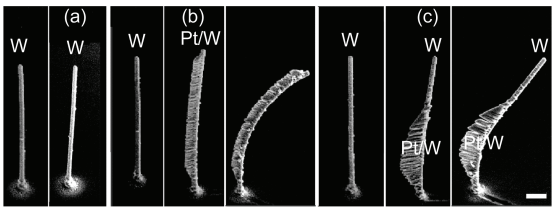

Figure 3 SEM images showing the bending of striped (type C) Pt/W nanowires: (a) W composite nanowires; (b) striped Pt/W nanostructures; and (c) partially striped Pt/W structure. In (a)–(c), the SEM iamge in the left hand side is for the as-deposited structure and that in the right hand side is for the annealed ones. The thermal annealing was taken in N_2 under T_A of 600°C, and the RTA duration is 60 s. (The scale bar is 1 μm).

was examined with type D nanowires that have various unit lengths. The length of each unit was changed using deposition time of 1, 2, 3 and 6 min for each material in Figures 4(a)–(d), respectively. The growth rate for the Pt composite portion was about 0.7 μm/min and it is about 0.2 μm/min for W composite. Besides, the unit properties can also be tuned using different gas precursors or by rotation of the sample stage. Figure 4 shows the SEM images of different segmented nanowire structures annealed at 500°C. The annealing time for each circle is 60 s, and the number of circle, *N*, is increased from 1 to 6 from left to right. It can be seen that for a smaller unit size, the bending is more arch-like and by increasing the annealing time, the extent of bending increased. This is similar to behavior of the FIB-grown gradient Pt nanowires and could be explained with the factor of difference in the expansion coefficients, which determines the degree of bending when either the RTA temperature or RTA cycle is increased [23]. For the Pt composite nanowire, the difference in the expansion coefficients increased with the annealing temperature, and consequently, resulted in bigger degree of bending.

Meanwhile, for nanowires with only one unit, the bending occurred only at the bottom portion of the nanowires (the part of Pt), and the total deviation from vertical was maximized. Since W has thermal expansion coefficient about half of that of the Pt, and under 500°C, W and Si alloys are not likely to be formed to cause inhomogeneous change of the volume. Therefore, FIB-grown W did not show any obvious bending at 500°C, the bending is mainly caused by the Pt segments, and the maximized bending for the one unit nanowire suggests that the W part could, to some extent, hold back the bending of the Pt portion, possibly due to any interfacial effect.

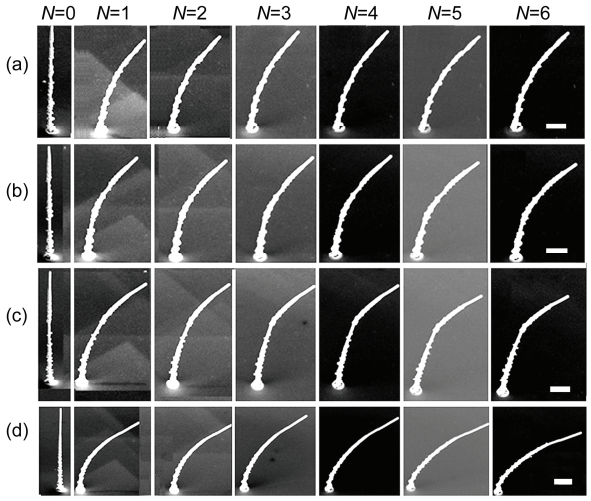

Figure 4 Deformation of segmented nanowires (type D) with various unit sizes. The length of W, and Pt composite in each segment is (0.2 μm, 0.7 μm), (0.4 μm, 1.4 μm), (0.6 μm, 2.1 μm), and (1.2 μm, 4.2 μm) for (a)–(d), respectively. The annealing time for each circle is 60 s, the number of annealing circle *N* is increased from 1 to 6 from left to right. The scale bar is 1 μm.

Also, various annealing temperatures were used to further explore the deformation process of W-Pt-segmented nanowires. In each unit, the deposition time for W and Pt segment is 1 min and the corresponding height for W and Pt is 0.2 and 0.7 μm, respectively. Figures 5(a)–(d) present the SEM image of the as-grown Pt-W nanowire structures and those annealed with T_A below 600°C. From these results, we can see that the time constant for the process of structural change, possibly caused by defects/elemental diffusion, recrystallization, and grain growth in the wire is of order of minutes. Therefore, the initial anneal was not long enough for the structure to reach its equilibrium at that temperature, in that further bending can be seen when more annealing cycles were performed. The saturation of the bending angle of nanowires may be understood in terms of the termination of the cluster growth. Both the RTA temperature and the number of cycles affect the cluster growth, hence the wire bending process. Different from the mild bending when T_A was below 600°C, an intriguing behavior, folding, rather than bending, was observed for segmented nanowires when the annealing temperature exceeded 700°C. Such a behavior suggests that fast heating caused sudden release of the strain through the weak point at the joint position, while defects or elemental diffusion, recrystallization, and grain growth were not the main factors that contribute to the bending when severe heat was applied in a short timescale. This behavior further indicates that folding of different segments by thermal annealing may be used as an approach for producing complicated 3D metallic nanostructures.

Also, two kinds of Pt-W-segmented nanowires were grown and the SEM image of the as-deposited nanostructures is shown in the left column Figure 6. The length for the Pt and W portions in the unit is about 1.5 and 0.5 μm, respectively. The Pt (R) and Pt (L) means that during growth, the gas precursor nozzle was placed on the right- and left-hand sides of the ion beam scanning position, respectively. The change in the relative position of the gas nozzle was achieved by rotating the sample stage by 180°. The thermal annealing was conducted at T_A of 500°C in N_2 for 60 s, and the number of circle, *N*, was increased from 1 to 6 from left to right. Although it can be seen that the for both kinds of structures, the bending increases with the annealing number of circles, the increment is smaller for

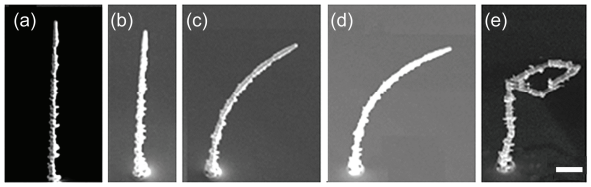

Figure 5 The annealing temperature dependent bending behaviors of W–Pt- segmented nanowire (type D): (a) as-grown; (b) T_A = 300°C; (c) T_A =500°C; (d) T_A =600°C; (e) T_A=700°C. The scale bar is 1 μm.

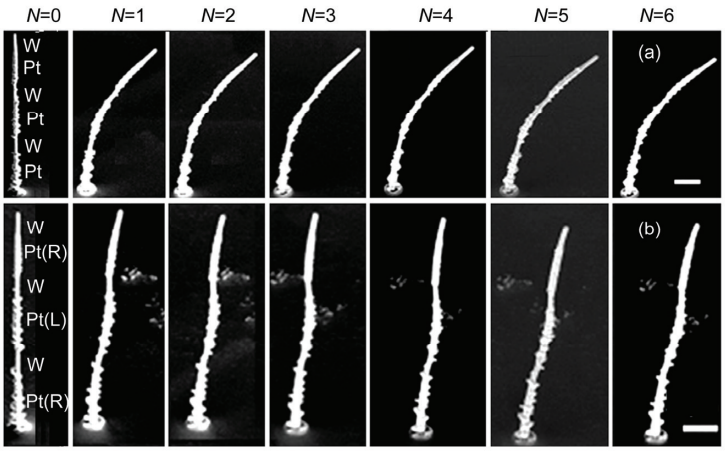

Figure 6 Deformation of segmented nanowires with different unit arrangements: (a) Regular stacking of Pt-W units, and the (b) reversed stacking of Pt–W units. The annealing was performed under 500°C and each circle took 60 s, and the number of annealing circles was increased from 1 to 6 from left to right. The scale bar is 1 μm.nanowire with Pt portions have different relative positions with respect to the gas precursor nozzle. These results suggest that besides the annealing conditions, the size and material type of the as-grown nanowires, the relative position of the strips, or the profile distribution direction of the gradient nanowires could also be used to control the bending direction for achieving complex 3D architectures.

nanowire with Pt portions have different relative positions with respect to the gas precursor nozzle. These results suggest that besides the annealing conditions, the size and material type of the as-grown nanowires, the relative position of the strips, or the profile distribution direction of the gradient nanowires could also be used to control the bending direction for achieving complex 3D architectures.

In summary, free-standing nanostructures were designed and fabricated through thermally induced shape modification based on FIB-deposited Pt gradient nanowires, striped Pt/W, and Pt-W-segmented nanowire structures. The thermally induced deformation was found to happen at temperatures ranging from 200°C up to 900°C, which could provide great flexibility for efficient fabrication of out-of-plane architectures based on various types of material systems. The gradient nanowires bent with perfect arc shape and the bending angle of the nanowire can be precisely controlled by growth parameters, the annealing temperature, and annealing duration/cycle. The host W nanowires bent only at the position with Pt composite deposited and the bending extent is determined by the size of the Pt deposit, similar to the Pt nanowire radius-dependent bending trends. Meanwhile, segmented nanowires bent in almost an arch shape when T_A is below 600°C, indicating mild and gradual possibly defects and elemental diffusion, recrystallization and grain growth in the wire, while fast heating with T_A suddenly exceeded 700°C, strain release through the weak point leading to regular folding at the joint position. These results indicated that thermally induced shape modification of free-standing nanowires can be effectively employed to construct 3D structures and form reliable contacts with potential for advanced functionalities. Although theoretic work and more experiments are required to reveal the mechanism behind the folding of the segmented nanowire upon thermal annealing, thermally annealing of hybrid structures could be a cost-effective approach for fabrication of complex 3D nanostructures for practical application in a wide field of applications, for example, mechanics, biology, and electronics.

This work was supported by the Outstanding Technical Talent Program of the Chinese Academy of Sciences and the National Natural Science Foundation of China (Grant Nos. 91123004, 11104334, 50825206, 10834012 and 60801043).

1 Ferain I, Colinge C A, Colinge J P. Multigate transistors as the future of classical metal-oxide-semiconductor field-effect transistors. Nature, 2011, 479: 310–316
2 Valentine J, Zhang S, Zentgraf T, et al. Three-dimensional optical metamaterial with a negative refractive index. Nature, 2008, 455: 376–379
3 Gouma P, Kalyanasundaram K, Xiao Y, et al. Nanosensor and breath analyzer for ammonia detection in exhaled human breath. Sensors J IEEE, 2010, 10: 49–53
4 Tian B Z, Karni T, Qing Q, et al. Three-dimensional, flexible nanoscale field-eEffect transistors as localized bioprobes. Science, 2010, 329: 830–834
5 Noda S, Tomoda K, Yamamoto N, et al. Full Three-dimensional photonic bandgap crystals at near-infrared wavelengths. Science, 2000, 289: 604–606
6 Romans E J, Osley E J, Young L, et al. Three-dimensional nanoscale superconducting quantum interference device pickup loops. Appl Phys Lett, 2010, 97: 222506
7 Zhang S, Fan W, Minhas B K, et al. Midinfrared resonant magnetic nanostructures exhibiting a negative permeability. Phys Rev Lett, 2005, 94: 037402
8 Fan K, Strikwerda A C, Tao H, et al. Stand-up magnetic metamaterials at terahertz frequencies. Opt Express, 2011, 19: 12619–12627
9 Burckel D B, Wendt J R, Ten Eyck G A, et al. Micrometer-scale cubic unit cell 3D metamaterial layers. Adv Mater, 2010, 22: 5053–5057
10 Chen C C, Hsiao C T, Sun S L, et al. Fabrication of three dimensional

split ring resonators by stress-driven assembly method. Opt Express, 2012, 20: 9415–9420
11 Rill M S, Plet C, Thiel M, et al. Photonic metamaterials by direct laser writing and silver chemical vapour deposition. Nat Mater, 2008, 7: 543–546
12 Gansel J K, Thiel M, Rill M S, et al. Gold helix photonic metamaterial as broadband circular polarizer. Science, 2009, 325: 1513–1515
13 Cui A, Li W, Luo Q, et al. Free-standing nanostructures for three-dimensional superconducting nanodevices. Appl Phys Lett, 2012, 100: 143106
14 Cui A, Li W, Luo Q, et al. Controllable three dimensional deformation of platinum nanopillars by focused-ion-beam irradiation. Microelectron Eng, 2012, 98: 409–413
15 Cui A, Fenton J C, Li W X, et al. Ion-beam-induced bending of free-standing amorphous nanowires: The importance of the substrate material and charging. Appl Phys Lett, 2013, 102: 213112
16 Luo J K, Huang R, He J H, et al. Modelling and fabrication of low operation temperature microcages with a polymer/metal/DLC trilayer structure. Sensors Actuators A-Phys, 2006, 132: 346–353
17 Py C, Reverdy P, Doppler L, et al. Capillary origami: Spontaneous wrapping of a droplet with an elastic sheet. Phys Rev Lett, 2007, 98: 156103
18 Lu Y W, Kim C J. Microhand for biological applications. Appl Phys Lett, 2006, 89: 164101
19 Jager E W H, Inganäs O, Lundström I. Microrobots for micrometer-size objects in aqueous media: potential tools for single-cell manipulation. Science, 2000, 288: 2335–2338
20 Iwase E, Shimoyama I. Multistep sequential batch assembly of three-dimensional ferromagnetic microstructures with elastic hinges. J Microelectromech Syst, 2005, 14: 1265–1271
21 Leong T G, Zarafshar A M, Gracias D H. Three-dimensional fabrication at small size scales. Small, 2010, 6: 792–806
22 Cui A, Li W, Shen T H, Yao Y, et al. Thermally induced shape modification of free-standing nanostructures for advanced functionalities. Sci Rep, 2013, 3: 2429
23 Utke I. Nanofabrication Using Focused Ion and Electron Beams: Principles and Applications. Oxford: Oxford University Press, 2012
24 Inkson B J, Dehm G. Thermal stability of Pt nanowires manufactured by Ga+ focused ion beam (FIB). In: Meldrum A, Roorda S, Bernas H, eds. Nanostructuring Materials with Energetic Beams. Warrendale, Pa.: MRS Online Proceedings Library, 2003. 777
25 Sheldon B W, Lau K H A, Rajamani A. Intrinsic stress, island coalescence, and surface roughness during the growth of polycrystalline films. J Appl Phys, 2001, 90: 5097–5103
26 Schmidt O G, Eberl K. Nanotechnology: Thin solid films roll up into nanotubes. Nature, 2001, 410: 168